*J. Fluid Mech.* (2005), *vol.* 543, *pp.* 137–146. © 2005 Cambridge University Press 
doi:10.1017/S0022112005006373 Printed in the United Kingdom

# Skipping stones

By LIONEL ROSELLINI[1], FABIEN HERSEN[1], CHRISTOPHE CLANET[1] AND LYDÉRIC BOCQUET[2]

[1]IRPHE, UMR 6594, 49 rue F. Joliot-Curie, BP 146, 13384 Marseille, France

[2]Laboratoire PMCN, UMR CNRS 5586, Université Lyon-I, 43 Bd du 11 Novembre 1918, 69622 Villeurbanne Cedex, France

(Received 5 April 2005 and in revised form 22 July 2005)

We first report a quantitative experimental study of the collision of a spinning disk with water, from a single to many skips. We then focus on the high spin limit and propose a simple model which enables us to discuss both the physical origin of the bounces and the source of the dissipation which fixes the number of skips.

## 1. Introduction

"One, two, three, four": this is the number of skips achieved by the stone in figure 1.

The rules of competition for skipping stones have never changed (Thomson 2000): a stone or a shell is thrown over a water surface and the maximum number of bounces distinguishes the winner. Part of the attraction of this game comes from the puzzling questions it raises: How can a stone bounce on water? How many skips can it achieve?

The impact of objects on water has been the object of a large amount of work in the literature (von Kármán 1930; Johnson & Reid 1975; Johnson 1998). Most of these works have focused (mainly due to military applications, e.g. Dambusters) on the impact of spherical and cylindrical objects, and clarified rebound conditions as a function of impact velocity. If $R$ characterizes the size of the object, $U$ its velocity and $\rho$, $\nu$, $\sigma$ the fluid properties (respectively density, kinematic viscosity and surface tension) all the above studies are in the limit of large Reynolds number ($Re \equiv UR/\nu \gg 1$) and large Weber number ($\rho U^2 R/\sigma \gg 1$) where inertial effects dominate both viscous and surface forces. Our study belongs to the same domain. However, even if the phenomena at play are similar in the case of stone skipping, the case of a flat (generally spinning) object like a stone is more difficult. In this latter case, a few theoretical analyses have attempted to extract the physical mechanisms (Stong 1968; Crane 1988; Bocquet 2003) and recently, three of us have published the first quantitative experimental results on the first bounce (Clanet, Hersen & Bocquet 2004). This study has motivated extensive numerical simulations (Nagahiro & Hayakawa 2005; Yabe *et al.* 2005). Here, we first complete our previous results by showing the skipping stone domain in a general phase diagram. Then, we extend the study to several skips and determine the origin of the dissipation responsible for the end of the skipping.

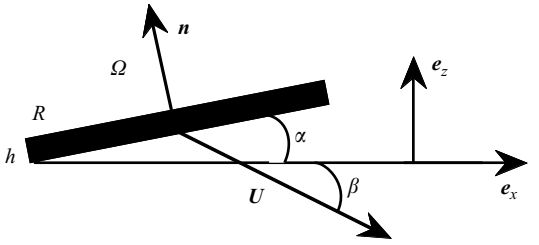
## 2. Experimental setup

The conventions used throughout the article are presented in figure 2: a model stone of thickness $h$ and radius $R$ has a translation velocity $\boldsymbol{U}$ and spinning velocity $\boldsymbol{\Omega} \equiv \Omega \boldsymbol{n}$, where $\boldsymbol{n}$ is the unit vector normal to its surface. The orientation of the

https://doi.org/10.1017/S0022112005006373 Published online by Cambridge University Press



FIGURE 1. Superposition of images showing, from left to right, the successive positions of a spinning stone during the first four skips.




| Stone | $R$ (mm) | $h$ (mm) |
|---|---|---|
| 1 | 25 | 2.75 |
| 2 | 25 | 5.55 |
| 3 | 50 | 2.75 |
| 4 | 50 | 5.55 |

FIGURE 2. Conventions used and geometrical properties of the disks.

.

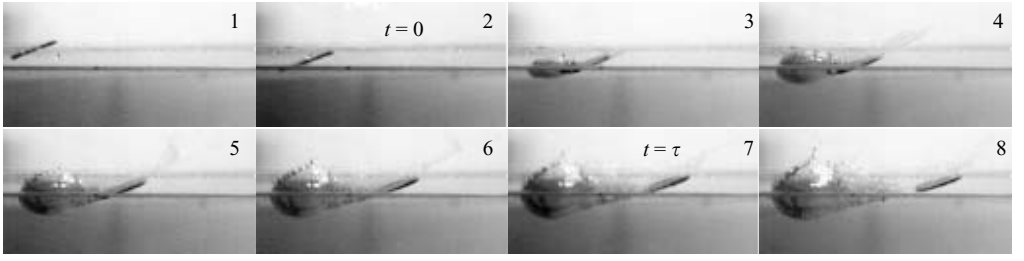



FIGURE 3. Chronophotography of a skipping stone, obtained with an aluminium disk of radius $R = 2.5$ cm, thickness $h = 2.75$ mm, translation velocity $U = 3.5\,\mathrm{m\,s^{-1}}$, angular velocity $\Omega = 65\,\mathrm{rot\,s^{-1}}$, attack angle $\alpha = 20°$, trajectory angle $\beta = 20°$. Time increases from left to right and from top to bottom with the time step $\Delta t = 6.5$ ms.

stone is defined by the attack angle $\alpha$ such that $\cos\alpha \equiv \boldsymbol{n}\cdot\boldsymbol{e}_z$, where $\boldsymbol{e}_z$ is the unit vector normal to the unperturbed water surface. The direction of motion of the stone is defined by the impact angle $\beta$ such that $\cos\beta \equiv \boldsymbol{U}\cdot\boldsymbol{e}_x$, where $\boldsymbol{e}_x$ is the unit vector tangent to the water surface.

An experimental setup has been designed to control independently $\Omega$, $U$, $\alpha$ and $\beta$. The collision of the stone with water is recorded using a high-speed video camera (Kodak HS4540). Most of the experiments are conducted with an aluminium stone, that is with the stone ($s$) to water ($w$) density ratio: $\rho_s/\rho_w \approx 2.7$. The geometrical characteristics of the stones are presented in figure 2.

## 3. Experimental results

### 3.1. *A single skip*

#### 3.1.1. *Chronophotography*

Chronophotography of a typical collision sequence is presented in figure 3. The collision time $\tau$ is measured on such graphs as the time during which the stone is in contact with water: as an example we measure $\tau \approx 32$ ms in figure 3. We also observe that under these conditions of large spin velocity, the attack angle $\alpha$ remains constant during the whole impact process. Finally, the cavity created is not symmetrical: it exhibits a larger curvature close to the impact.

https://doi.org/10.1017/S0022112005006373 Published online by Cambridge University Press

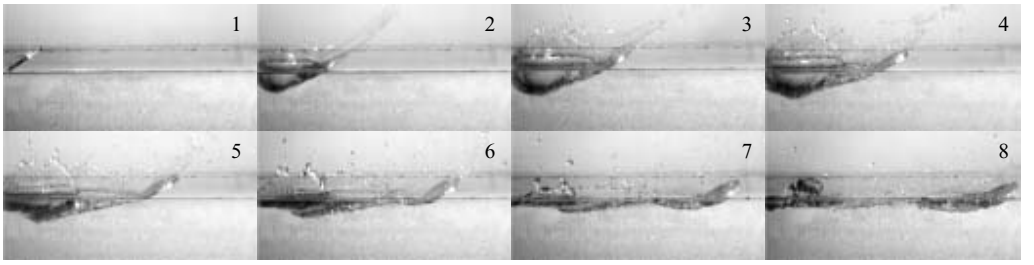



FIGURE 4. Chronophotography of a surfing stone, obtained with an aluminium disk with $R = 2.5$ cm, $h = 2.75$ mm, $U = 3.5\,\mathrm{m\,s^{-1}}$, $\alpha = 30°$, $\beta = 35°$, $\Omega = 65\,\mathrm{rot\,s^{-1}}$. The time step between each image is $\Delta t = 8.9$ ms.

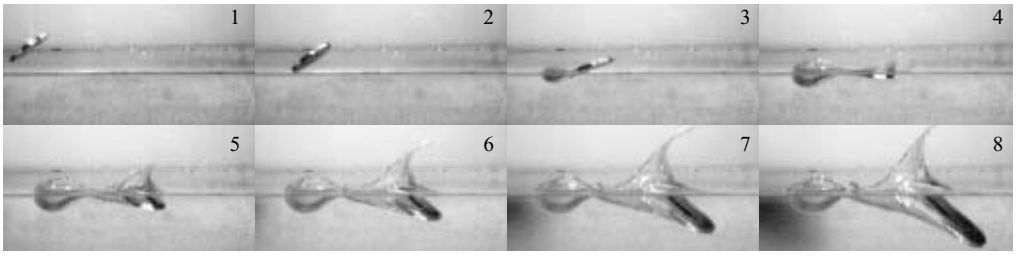



FIGURE 5. Chronophotography of a diving stone, obtained with an aluminium disk with $R = 2.5$ cm, $h = 2.75$ mm, $U = 3.5\ \mathrm{m\ s^{-1}}$, $\alpha = 35°$, $\beta = 20°$, $\Omega = 0\,\mathrm{rot\,s^{-1}}$. The time step between each image is $\Delta t = 8.9$ ms.

### 3.1.2. *Surfing*

The collision sequence repeated in a 'self-similar' way until the parameters at the impact (angles and velocity) prevent the stone escaping from the water and force it to surf. This surfing regime is illustrated in figure 4. We observe in this sequence that the angle $\alpha$ remains constant over the sequence as in figure 3, but the stone, even though it oscillates vertically, never detaches from the water.

### 3.1.3. *Effect of spin*

The spin velocity has a strong influence on the collision, in particular via its effect on the attack angle $\alpha$. This is illustrated in figure 5, where $\Omega = 0$: without any rotation, the stone tumbles at the impact and dives into the pool. The main effect of spin is thus to stabilize the stone during the impact, through the gyroscopic effect (Bocquet 2003).

More quantitatively, we present in figure 6($a$) the measured collision time $\tau$ as a function of spin velocity $\Omega$. This curve exhibits a strongly enhanced collision time at small spin velocity $\Omega$, emphasizing the absence of a rebound in the $\Omega \to 0$ limit. In the other limit of large spin velocity, the collision time is observed to reach a saturation value (of the order of 30 ms), indicating that the disk is fully stabilized by the gyroscopic effect.

This effect can be rationalized by introducing the Rossby number, $Ro = \Omega\tau$, which compares the rotation time to the contact time. In the large spin velocity regime ($Ro \gg 1$), the attack angle $\alpha$ is constant and equal to its initial value, as observed in figures 3 and 4. According to figure 6($a$), stabilization occurs for $Ro \geqslant 1$.

https://doi.org/10.1017/S0022112005006373 Published online by Cambridge University Press

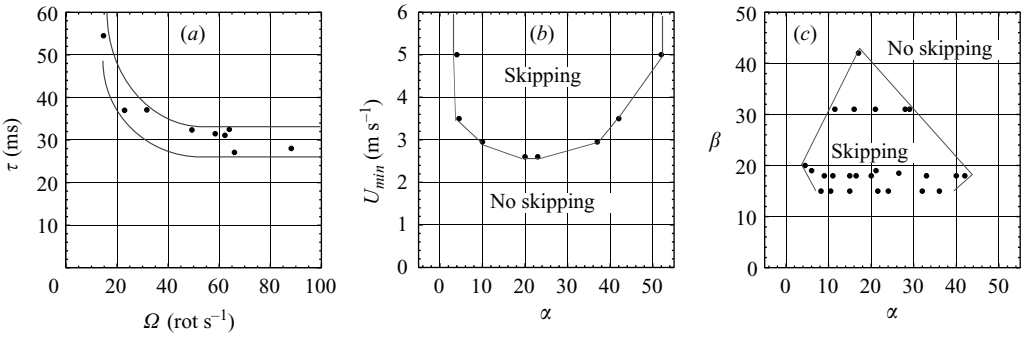



FIGURE 6. (*a*) Evolution of the collision time $\tau$ with the spinning velocity $\Omega$ for $U = 3.5\,\mathrm{m\,s^{-1}}$, $\alpha = 20°$, $\beta = 20°$. (*b*) Domain of the skipping stone in the $\{\alpha, U_{min}\}$ plane with $\Omega = 65\,\mathrm{rot\,s^{-1}}$, $\beta = 20°$. (*c*) Domain of the skipping stone in the $\{\alpha, \beta\}$ plane with, $\Omega = 65\,\mathrm{rot\,s^{-1}}$, $U = 3.5\,\mathrm{m\,s^{-1}}$. In $R = 2.5$ cm, $h = 2.75$ mm (*a–c*) the continuous lines are to guide the eye.

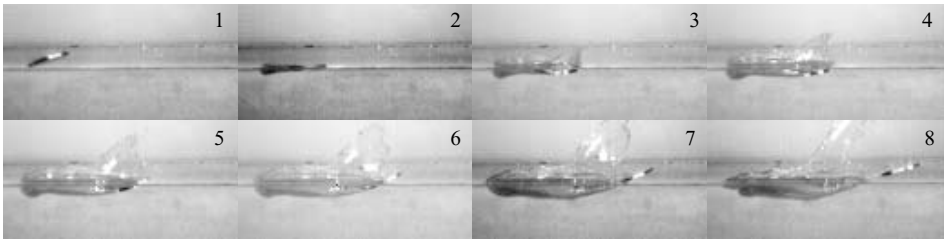



FIGURE 7. Chronophotography of a skipping stone in an intermediate rotation regime: $R = 2.5$ cm, $h = 2.75$ mm, $U = 3.5\,\mathrm{m\,s^{-1}}$, $\alpha = 20°$, $\beta = 18°$, $\Omega = 10\,\mathrm{rot\,s^{-1}}$. The time step between each image is $\Delta t = 8.9$ ms.

### 3.1.4. *Intermediate rotation rate: the 'trout' regime*

For intermediate rotation rates, the stone can bounce although its angle with the surface changes during the impact. We have called this the 'trout' regime and it is illustrated in figure 7. In this figure, we observe that the initial inclination of the stone ($\alpha = 20°$) decreases at the impact to almost $\alpha = 0$ (pictures 2 and 3). Then it increases and allows the stone to bounce (figure 8). Here, we clearly have a coupling between the cavity created at the impact and the angle $\alpha$ of the stone. In the remaining part of this paper we restrict our study to the high spin regime: $Ro \gg 1$.

### 3.1.5. *Dynamical phase diagram*

With the three remaining control parameters, $\{U, \alpha, \beta\}$, a dynamical phase diagram can be constructed, highlighting the conditions for a successfull bounce (the 'skipping stone' domain). Cross-sections in the $\{U, \alpha\}$ and $\{\alpha, \beta\}$ variables are shown in figures 6(*b*) and 6(*c*). Unexpectedly this phase diagram points out the specific role played by the value $\alpha \simeq 20°$: the lowest velocity for a rebound, $U_{min}$, reaches a minimum ($U_{min} \approx 2.6\,\mathrm{m\,s^{-1}}$) for $\alpha \simeq 20°$, while the maximal successful domain in $\beta$ is also achieved for this specific value of $\alpha$. One may also observe that no rebound is possible for impact angles $\beta$ larger than 45°. In these 'no rebound regions', the stone is observed to surf as in figure 4. We report in figure 8(*a*) the experimental measurements for the collision time for a given stone at different speed and angle $\beta$. The main feature on this plot is the existence of a minimal value of the collision time $\tau_{min}$ again obtained for $\alpha \simeq \alpha_{min} = 20°$.

https://doi.org/10.1017/S0022112005006373 Published online by Cambridge University Press

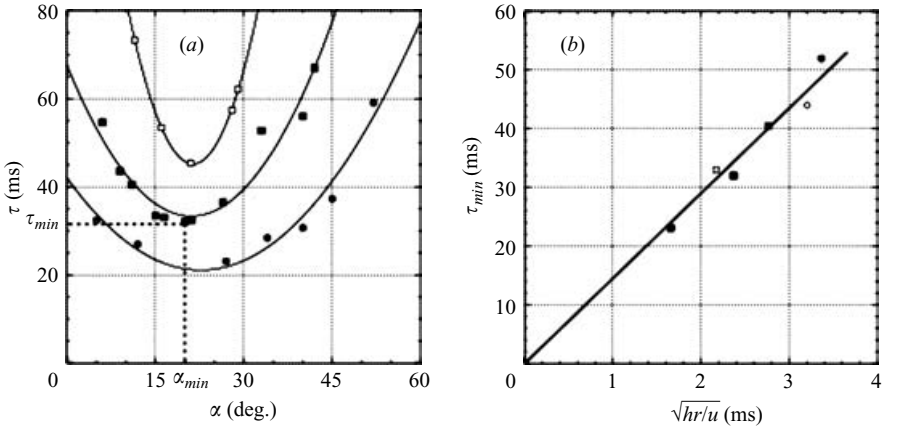



FIGURE 8. (*a*) Evolution of the collision time $\tau$ as a function of the attack angle $\alpha$ for $R = 2.5$ cm, $h = 2.75$ mm and different conditions: ■, $U = 3.5\ \mathrm{m\,s^{-1}}$, $\beta = 20°$; □, $U = 3.5\ \mathrm{m\,s^{-1}}$, $\beta = 30°$, ●, $U = 5\ \mathrm{m\,s^{-1}}$, $\beta = 20°$. (*b*) Evolution of the minimal contact time $\tau_{min}$ with the characteristic time scale $\sqrt{hR}/U$ with $\beta = 20°$ and $\alpha \approx 20°$ and different stones: ■, $R = 2.5$ cm, $h = 2.75$ mm; □ , $R = 5$ cm, $h = 2.55$ mm; ●, $R = 2.5$ cm, $h = 5.55$ mm; ○, $R = 5$ cm, $h = 5.55$ mm; the solid line present the results obtained numerically through the integration of equation (4.5).

In order to understand more specifically the physical mechanisms at play, we studied the evolution of this minimal collision time $\tau_{min}$ as a function of velocity $U$ for different stone diameters and thicknesses. As indicated in figure 8(*b*), the minimal contact time is found to follow the scaling, $\tau_{min} \propto \sqrt{hR}/U$ (for fixed $\alpha \approx 20°$ and $\beta = 20°$). This scaling is suggested by dimensional analysis: since the lift force $F_{lift}$ is the key aspect in the rebound process, a collision time can be constructed as $\tau \sim \sqrt{mR/F_{lift}}$ with $m$ the mass of the stone. This scaling is obtained using Newton's second law with $R/\tau^2$ as the characteristic acceleration. Now for the velocities under consideration, the Reynolds number is quite large ($Re = UR/\nu \sim 10^5$, with $\nu$ the kinematic viscosity of water) and the lift force is expected to scale as $F_{lift} \sim \rho_w S_{wetted} U^2$, where $S_{wetted} \sim \pi R^2$ (Landau & Lifshitz 1959). Using $m = \rho_s h \pi R^2$, one gets $\tau \propto \sqrt{hR}/U$, as is measured experimentally in figure 8(*b*).

### 3.2. *Many skips*

We now turn to the observation of a complete skipping stone sequence as presented in figure 1.

#### 3.2.1. *Velocity U and attack angle β*

In figures 9(*a*) and 9(*b*) we present the values of the horizontal velocity $U_x$ and attack angle $\beta$ after the impact as a function of their value before the impact (transfer function). This transfer function is particularly relevant for the skipping stone problem since the velocity and attack angle after a given collision are equal to the initial velocity and attack angle for the next collision: this property is due to the parabolic flight between two collisions (air friction being negligible).

An important point which emerges from figure 9(*a*) is that the horizontal component of the velocity barely changes over the collisions. On the other hand the attack angle exhibits a strong variation and decreases continuously over the collisions. This observation suggests that only the vertical ($z$) component of the velocity of the stone is strongly affected during the collision.

https://doi.org/10.1017/S0022112005006373 Published online by Cambridge University Press

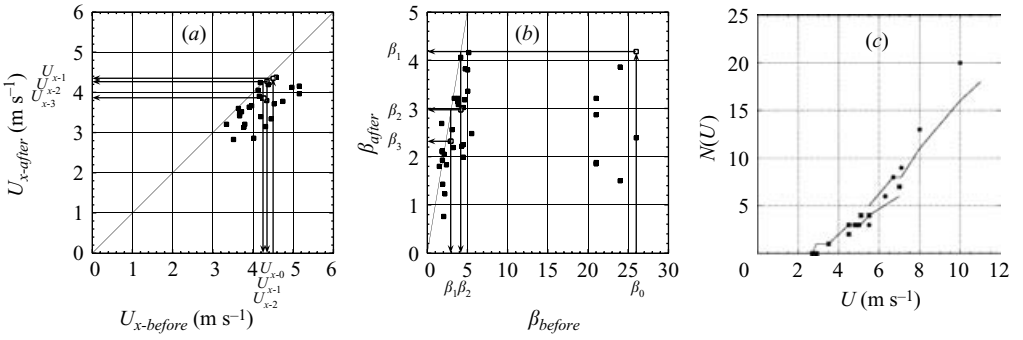



FIGURE 9. (*a*) Transfer function of the horizontal component of the velocity $U_x$ for stone 1 and different values of $\alpha$ (either 7° or 20°) and different values of $\beta$ (ranging from 20° to 26°). The example marked with the white squares has been obtained with $\alpha = 7°$ and $\beta = 26°$. (*b*) Transfer function of the angle $\beta$ for stone 1 and different values of $\alpha$ (either 7° or 20°) and different values of $\beta$ (ranging from 20° to 26°). The example marked with the white squares has been obtained with $\alpha = 7°$ and $\beta = 26°$ and $U = 4.5$ m s$^{-1}$. (*c*) Number of skips as a function of the initial velocity for stone 1 and $\alpha = 7°$ and $\beta = 20°$ (■), $\alpha = 10°$ and $\beta_0 = 9°$ (●). The continuous lines are the theoretical predictions obtained with the parameters of the experiment: $\alpha = 7°$ and $\beta_0 = 20°$(bottom line) and $\alpha = 10°$ and $\beta_0 = 9°$ (top line).

### 3.2.2. *Number of skips*

In figure 9(*c*) we present the evolution of the number of skips as a function of the initial velocity. In the present velocity regime, this number is basically a linear function of the velocity, above the minimum velocity introduced in figure 6(*b*).

## 4. Theoretical model of the collision process

### 4.1. *Towards a simple mechanical approach*

#### 4.1.1. *The hydrodynamic lift force on the disk*

The crucial ingredient of the description is the hydrodynamic force acting on the disk. For the velocities under consideration here ($U \sim$ m s$^{-1}$) the Reynolds number ($Re \equiv UR/\nu$) is of the order of $10^5$. In this potential flow limit, the reaction of the water on the stone is expected to take the form (von Kármán 1930; Landau & Lifshitz 1959)

$$\boldsymbol{F}_L = C_L \rho_w U^2 S_{wetted} f(\alpha, \beta)\boldsymbol{n} \tag{4.1}$$

where $S_{wetted}$ is the disk area in contact with water, $C_L$ the lift coefficient, and $f(\alpha, \beta)$ a non-dimensional function which contains the angular dependence of the lift force.

The difficult part is to propose a consistent description of the function $f(\alpha, \beta)$. Let us first note that this function is expected to depend on the total angle $\gamma = \alpha + \beta$, which is the relative angle between the water stream and the stone. Furthermore, symmetry considerations suggest that the function $f(\gamma)$ should be odd in $\gamma$ (one expects it to change sign around $\gamma = 0$). We have conducted complementary experiments to measure the lift force on a disk in a water stream, as described in the Appendix, and suggest the following expression for the force:

$$\boldsymbol{F}_L = \tfrac{1}{2}\rho_w U^2 S_{wetted} \sin(\alpha + \beta)\boldsymbol{n}. \tag{4.2}$$

As a by-product of these experiments, the dependences on the wetted area $S_{wetted}$ and velocity $U$ have been confirmed. The value $C_L \simeq 0.5$ is also provided by the experiments, which is the same as found by Glasheen & McMahon (1996).

https://doi.org/10.1017/S0022112005006373 Published online by Cambridge University Press

### 4.2. *Some qualitative remarks*

A few comments can be made on the limit $\alpha, \beta \ll 1$. This limit is often achieved after the first collision where $|\beta|$ takes a small value, that is tangent to the water surface (see figure 1). In this limit the horizontal force reduces to $F_x \approx 0.5\rho_w U^2 S_{wetted}(\alpha+\beta)\alpha$. One deduces that $F_x$ is order 2 in $\alpha$ which implies that the momentum in the $x$-direction is weakly affected during the collision. This is qualitatively observed in figure 9($a$).

Along the $z$-direction, $F_z \approx 0.5\rho_w U^2 S_{wetted}(\alpha+\beta)$, from which $F_z$ is first order in $\alpha$, contrary to $F_x$ which is second order. The momentum evolution in the $z$-direction is thus faster than in the $x$-direction. Moreover, the $\alpha+\beta$ dependence implies that, at a given $z$ location, $F_z$ is larger in the downgoing phase ($\beta > 0$) than in the upgoing one ($\beta < 0$). This difference in the value of the reaction force is the physical origin of the asymmetry of the air cavity and of the dissipation (see § 4.4).

For the gyroscopic stabilization, the Euler equations for the symmetrical top (Bocquet 2003) lead to the evaluation of the relative inclination of the stone at the impact: $\delta\alpha/\alpha \sim F.R/(mR^2\Omega^2)$. Using the expression for the force $F$, we get: $\delta\alpha/\alpha \sim (\rho/\rho_s)U^2/(Rh\Omega^2)$. The stabilization of the stone ($\delta\alpha/\alpha \ll 1$) is thus expected in the limit $Ro \gg \sqrt{\rho/\rho_s}$ (using the previous estimate of the collision time, $\tau \sim \sqrt{hR}/U$ to define $Ro$).

### 4.3. *Equations of motion*

The equation of motion we integrate to get the stone trajectory is

$$m\frac{\mathrm{d}U}{\mathrm{d}t} = K\ 0.5\rho_w U^2 S_{wetted}\sin(\alpha+\beta)\boldsymbol{n} + m\boldsymbol{g}. \tag{4.3}$$

The velocity is given by $U^2 = U_x^2 + U_z^2$ and $g$ is the acceleration due to gravity. The constant $K = 1$ when the stone touches the water and is zero while it is in the air. In (4.3) the wetted area $S_{wetted}$ depends on the immersed depth $z$ and thus varies during the collisional process. For a circular stone, the immersed area is given in terms of the area of a truncated circle as

$$S_{wetted}(s) = R^2[\cos^{-1}(1-s/R) - (1-s/R)\sqrt{1-(1-s/R)^2}], \tag{4.4}$$

where $s = |z|/\sin\alpha$ is the maximum immersed length (Bocquet 2003). Initial conditions for the equation of motion, (4.3), fix the initial velocity $U = (U_x(t=0)^2 + U_z(t=0)^2)^{1/2}$ and angle $\beta_0 = \tan^{-1}(-U_z(t=0)/U_x(t=0))$. By convention $z(t=0) = 0$. Note that in the present high spin velocity limit, the angle $\alpha$ remains almost constant during the collision. This is different for the angle $\beta$, which is related to the direction of the velocity with respect to the horizontal, $\beta = \tan^{-1}(-U_z(t)/U_x(t))$. Since the stone moves up and down, this angle does vary over the collision time, and changes sign.

The nonlinear equation (4.3) can be solved numerically. The first interesting result obtained from this description is that a minimum velocity $U_{min}$ is required for the stone to rebound. Mathematically speaking this corresponds to a situation where the stone is able to come back to its initial depth ($z = 0$). For $U > U_{min}$ the depth $z(t)$ of the stone returns to its initial value $z = 0$ after a finite (collision) time. On the other hand, for $U < U_{min}$, the depth $z$ always remains negative and the stone is unable to return to the water surface. We plot in figure 10($a$) the minimum velocity obtained through the numerical integration of equation (4.3). Despite the simplicity of the model, this figure reveals a good agreement between the experimental results and the numerical ones. A similar agreement is found for the collision times, as shown in figure 10($b$), and for the stone-skipping domain, see figure 10($c$). This indicates that

https://doi.org/10.1017/S0022112005006373 Published online by Cambridge University Press

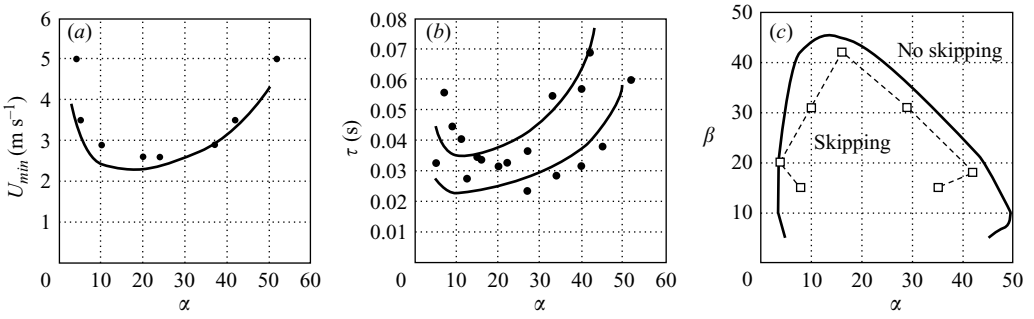



FIGURE 10. (*a*) Minimum velocity as a function of $\alpha$ for $\beta = 20°$ and (*b*) collision time. The solid lines are the theoretical prediction (see text). (*c*) Domain of the skipping stone: comparison between experimental results (–□–) and theoretical prediction (solid line). Parameters are similar to those in figure 6(*c*).

the model is able to capture the physical mechanisms at play during the stone–water collision.

It is easy to obtain the total number of skips for given initial velocity $U$, and angles $\alpha$, $\beta$. After a given collision, numbered as $n$, both the velocity and angle $\beta$ are computed at time $t = \tau$, with $\tau$ the collision time. These values are then taken as input for the initial conditions for the next, $n+1$, collision. This process is repeated until the stone is unable to bounce. The predictions of this description are plotted against the experimental results in figure 9(*c*). Again, the agreement is seen to be good.

### 4.4. *Source of dissipation*

We now focus more precisely on the origin of the dissipation, responsible for the end of bouncing. This discussion relies on the following observations: the horizontal velocity barely varies over the collisions (especially in the small-$\alpha$ limit), while the angle $\beta \equiv \tan^{-1}(-V_z(t)/V_x(t))$ decreases over the collisions. Assuming $V_x(t) \approx U$, one obtains for small angles $\beta \simeq -V_z(t)/U$. These observations allow a simplified analysis of the motion along the $z$-axis:

$$m\frac{\mathrm{d}U_z}{\mathrm{d}t} = F_L^z - mg. \tag{4.5}$$

The projection of lift force along $z$ becomes

$$F_L^z = \tfrac{1}{2}\rho_w U^2 S_{wetted}(z) f(\alpha+\beta)\cos(\alpha). \tag{4.6}$$

Now for small angles $\beta$, one may write $f(\alpha+\beta) \simeq f^{(0)}(\alpha) + f^{(1)}(\alpha)\beta$, with in the present disk geometry $f^{(0)}(\alpha) = \sin(\alpha)$ and $f^{(1)}(\alpha) = \cos(\alpha)$. Using $\beta \simeq -V_z(t)/U$, one obtains eventually $F_L^z = F^{(0)}(z) - \zeta(z)V_z$ with $F^{(0)}(z) = \frac{1}{2}\rho_w U^2 S_{wetted}(z)\ f^{(0)}(\alpha)\ \cos(\alpha)$, and $\zeta(z) = \frac{1}{2}\rho_w U S_{wetted}(z)\ f^{(1)}(\alpha)\ \cos(\alpha)$.

The parameter $\zeta$ plays the role of an *effective friction coefficient*. This is more explicit when rewriting the equation of motion along $z$:

$$m\frac{\mathrm{d}V_z}{\mathrm{d}t} = F^{(0)}(z) - \zeta(z)V_z - mg. \tag{4.7}$$

This equation takes the form of a *damped nonlinear oscillator*. This shows that the velocity along $z$, hence $\beta$, will decrease over the collisions. This can be verified

https://doi.org/10.1017/S0022112005006373 Published online by Cambridge University Press

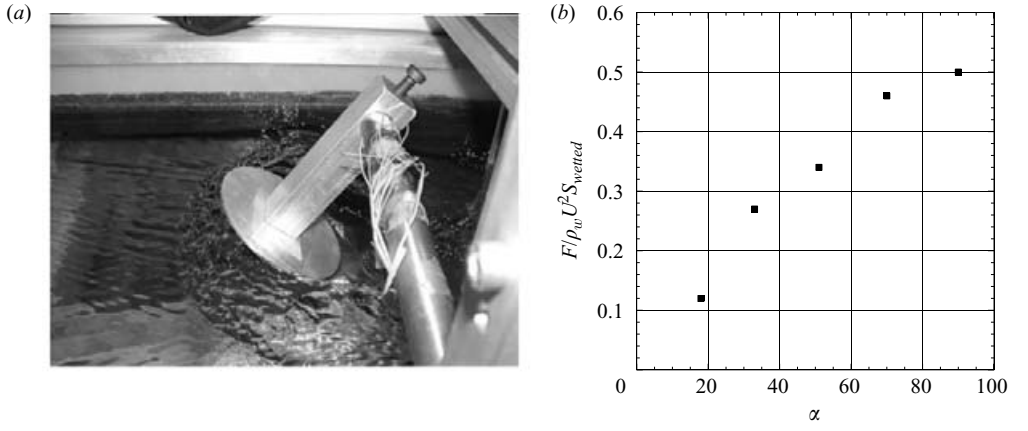



FIGURE 11. (*a*) Picture of the experiment conducted to measure the reaction force of the water. (*b*) Quantitative evolution of the reduced force $F/(\rho_w U^2 S_{wetted})$ as a function of $\alpha$.

explicitly by computing the '$z$-energy' dissipation from (4.7) over a collision time $\tau$:

$$\tfrac{1}{2}m\left[V_z^2\right]_{\text{final}} - \tfrac{1}{2}m\left[V_z^2\right]_{\text{initial}} = -\int_0^\tau \mathrm{d}t\ \zeta(z)V_z^2(t). \tag{4.8}$$

This also indicate that in order to bounce the initial '$z$-kinetic energy' $\frac{1}{2}m[V_z^2]_{\text{initial}}$ has to be larger than the dissipated energy : $\frac{1}{2}m[V_z^2]_{\text{initial}} > \int_0^\tau \mathrm{d}t\ \zeta(z)V_z^2(t)$. This condition is at the origin of the existence of a threshold minimum velocity for the stone to bounce (see figure 10) and correctly obtained through the numerical integration of equation (4.3). Globally, the stone does not stop because its initial kinetic energy is lost (since $V_x$ is barely modified over the skips). Rather, dissipation originates more subtly from the dependence of the lift force on the attack angle $\beta$, leading to a decrease of only the vertical component of the velocity over the collisions, up to its minimum threshold value.

## 5. Conclusion

Our study has highlighted the physical mechanisms involved in the skipping-stone phenomenon. In the high spinning velocity regime, we have shown that the stone bounces due to the hydrodynamic response of the water and that the source of dissipation lies in the dependence of this reaction force on the angle between the water surface and the trajectory of the stone. A natural extension of this study would be to examine the 'trout' regime, where a coupling between translation and spin effects is expected.

## Appendix. Measurements of the lift force on a disk

The lift is measured experimentally, using the setup presented in figure 11(*a*): a disk with fixed orientation is partially immersed at a fixed depth into a water stream, with known velocity. The force on the disk is measured thanks by a gauge. In this geometry, both the angle $\alpha$ and the relative velocity $U$ can be varied. Conversely the angle $\beta$ is here equal to zero. The stream velocity is typically of the order of $1\,\mathrm{m\,s^{-1}}$.

https://doi.org/10.1017/S0022112005006373 Published online by Cambridge University Press

The experimental results for the lift force are summarized in figure 11($b$): these experiments are well described by $F_L = \frac{1}{2}\rho_w V^2 S_{wetted} \sin(\alpha)$. Assuming that the lift force depends on the angles $\alpha$ and $\beta$ via the combination $\alpha + \beta$, this leads to the final results for the lift force

$$F_L = \tfrac{1}{2}\rho V^2 S \sin(\alpha + \beta). \tag{A 1}$$

## REFERENCES


Bocquet, L. 2003 *Am. J. Phys.* **71**, 150–155.

Clanet, C., Hersen, F. & Bocquet, L. 2004 *Nature* **427**, 1 Jan. 2004, p. 29.

Crane, H. R. 1988 *Phys. Teach.* **26**, 300–301.

Glasheen, J. W. & McMahon, T. A. 1996 *J. Expl Biol.* **199**, 2611.

Johnson W. 1998 *Intl J. Impact Enging* **21**, 15–24, 25–34.

Johnson, W. & Reid, S. R. 1975 *J. Mech. Engng Sci.* **17**, 71.

von Karman, Th. 1929 The impact of sea planes during landing. *NACA Tech. Note* 321. This paper can be downloaded from http://naca.larc.nasa.gov/reports/1929/naca-tn-321/naca-tn-321.pdf

Landau, L. D. & Lifshitz, E. M. 1959 *Fluid Mechanics*, pp. 168–175. Pergamon.

Nagahiro, S. I. & Hayakawa, Y. 2005 *Phys. Rev. Lett.* **94**, 174501.

Stong, C. L. 1968 *Sci. Am.* **219**, 112–118.

D'Arcy Thomson 2000 *Alliage* **44**, 77–78.

Yabe, T., Takizawa, K., Chino, M., Imai, M. & Chu, C. C. 2005 *Intl J. Numer. Meth. Fluids* **47**, 655–676.


https://doi.org/10.1017/S0022112005006373 Published online by Cambridge University Press